Progress In Electromagnetics Research, Vol. 118, 441–459, 2011

ATTENUATION IN EXTENDED STRUCTURES COATED WITH THIN MAGNETO-DIELECTRIC ABSORBER LAYER

M. Y. Koledintseva[1,*], A. G. Razmadze[1], A. Y. Gafarov[1], V. V. Khilkevich[1], J. L. Drewniak[1], and T. Tsutaoka[2]

[1]Missouri University of Science & Technology, Electrical and Computer Engineering Department, 115 EECH, Rolla, Missouri 65409, USA

[2]Hiroshima University, Higashi-Hiroshima 739-8524, Japan

Abstract—Thin absorbing layers containing magnetic alloy or ferrite inclusions can be effectively used for attenuating common-mode currents on extended structures, such as power cords, cables, or edge-coupled microstrip lines. An analytical model to evaluate attenuation on the coaxial line with the central conductor coated with a magneto-dielectric layer is proposed and validated by the experiments and numerical modeling. The analytical model is validated using available magneto-dielectric samples of different thicknesses. This model can serve for comparing and predicting the absorptive properties of different samples of magneto-dielectric materials, whose compositions may be unknown, but dielectric and magnetic properties can be determined by independent measurements over the specified frequency ranges. From modeling the absorption in a coaxial line with a wrapped central conductor, it could be concluded whether it is reasonable to use this particular material in such applications as a shield on an Ethernet or other cable, for reducing potential common-mode currents and unwanted radiation in the frequency range of interest.

1. INTRODUCTION

Composite thin sheet materials containing magnetic inclusions can be effectively used for electromagnetic noise-suppressing purposes and for solving numerous electromagnetic compatibility and immunity problems [1–4]. For example, thin absorbing magneto-dielectric layers

Received 30 May 2011, Accepted 30 June 2011, Scheduled 13 July 2011

* Corresponding author: Marina Y. Koledintseva (marinak@mst.edu).

suppress common-mode currents on extended structures, such as power cords, cables, or edge-coupled microstrip lines. They can also be used as patches on the conducting surfaces, e.g., on the walls of cavities and shielding enclosures. These composite materials may contain either randomly oriented and distributed, or aligned ferrite [5–9], ferromagnetic [10, 11], or artificial magnetic inclusions. The latter may be made of micro/nanowires, e.g., metasolenoids [12].

Electromagnetic absorbing effectiveness of materials is typically characterized and tested in terms of the shielding effectiveness (S.E.), which shows the attenuation of electric and/or magnetic fields by an absorbing layer of particular thickness [13, 14]. Another characteristic is the reflection loss (R.L.), which is calculated if the material is backed-up by a metal screen [1, 2]. However, characterization in terms of S.E. and R.L., strictly speaking, is applicable only to far fields and radar absorbing materials (RAM) [15]. For the purposes of electromagnetic compatibility/electromagnetic immunity (EMC/EMI), in which near fields are also of importance, evaluation of absorbing materials using frequency dependences of S.E. and/or R.L. is not sufficient [16]. Engineers encountering EMC/EMI problems in their designs may need information on what attenuation for electric and magnetic fields, or electromagnetic power is produced due to the certain amount of an absorbing material — per-unit-length (in cable applications), per-unit-area, or even per-unit-volume (in cavity/enclosure patch applications). They need to know how much absorbing material to take to achieve sufficient mitigation of noise, i.e., unwanted radiation or coupling.

When designing or choosing an appropriate absorbing material from a number of available candidates, a simple experiment-based technique to evaluate absorbing properties of the materials under test is desirable. This may be an evaluation of the per-unit-length attenuation of propagating waves in a transmission line or waveguide structure, whose cross-section is completely or partially filled with the material under test. If a thin sheet noise-suppressing material coats an extended metallic structure, e.g., a long metallic wire or a cable, the reduction of the radiation efficiency of this structure due to the suppression of the common-mode currents can be evaluated and correlated with the absorption properties of this material per geometrical unit.

An approach to evaluate and compare absorptive properties of different materials is considered in this paper. It is proposed to wrap the central conductor of an air-filled coaxial line with a thin layer of the test material and measure S-parameters on the line, retrieving the attenuation due to the material. The coaxial airline with the removable central conductor can be used — the same as is used for measuring permittivity and permeability of materials by the Nicolson-

Ross-Weir (NRW) technique [17–19]. In the latter, a washer-shaped test sample completely fills the cross-section of the coaxial line [20]. In the case of a very thin sheet material under test, the method described in [21] can be used. There are some other techniques to measure permittivity and permeability of thin sheet magnetic materials, but their description is beyond the scope of this paper. The good review of different measurement techniques is given in [22].

The physical mechanism of the wave attenuation in the air-filled line is an appearance of surface impedance on the metal surface that contributes to the loss along the line. In the other words, the presence of a thin magneto-dielectric layer upon a conductor surface contributes to the degradation of its effective conductivity. This is analogous to the power loss due to rough conductor interfaces [23–26].

An analytical solution of the problem of finding complex propagation constant and corresponding complex surface impedance associated with TM_z mode propagating along a coaxial line with a coated central conductor is presented herein. The frequency characteristics of permittivity and permeability of a thin magneto-dielectric layer coating the central conductor are supposed to be known. They can be measured using one of the known techniques, e.g., the NRW method. The proposed analytical model is based on matching boundary conditions for the vector electric and magnetic potentials in a layered structure [27], and rigorous solution of the resulting transcendental equation for wave numbers within the lossy magneto-dielectric layer coating the metal [28, 29]. The attenuation of quasi-TEM-mode in the air-filled coaxial line with the coated central conductor is analyzed based on the concept of surface displacement, introduced in [23]. The effective RLGC parameters of the structure, different from those in a lossless or low-loss air-filled coaxial line [30], are then extracted. The S-parameters for a section of the coaxial line with the coated central conductor then can be calculated using the transition from the RLGC parameters to the ABCD matrix parameters [31]. Using this model, a few examples of absorbing materials are tested, and frequency dependences of attenuation are shown. This analytical approach allows for comparing absorptive properties of different thin sheet magneto-dielectric materials. It also allows for simple comparing absorption level when using the same material, but of different thickness or length on the conductor. The analytical results for the transmission coefficient (S_{21}) are also compared with numerical simulations using the finite-element method (FEM) in CST Microwave Studio.

2. ANALYTICAL MODEL

Surface currents on a conducting surface are always induced by magnetic fields present in the vicinity of the metallic surface. In turn, the surface currents produce magnetic fields, which may be undesirable, especially if there are sharp edges, wedges, or slots. Fringing magnetic fields may contribute to unwanted coupling and radiation [32]. To suppress these surface currents, coating metal surfaces with materials possessing the sufficient magnetic loss in the frequency range of interest may be a solution.

An approach presented herein is based on the concepts of the surface impedance and surface displacement [23]. If there is a perfect electric conductor (PEC) and no absorbing coating, no skin effect will occur, tangential components of electric and normal component of magnetic field vectors will be zero, finite surface currents will flow on the PEC, and surface impedance zero will be zero. If the metallic surface is a non-perfect electric conductor (NPEC), the electromagnetic field will penetrate inside the conductor due to the skin-effect. Then the longitudinal electric field component will be non-zero. This will lead to the appearance of the surface impedance associated with the skin-depth. If metal surface is periodically rough or coated with a lossless dielectric layer, the surface impedance will be pure inductive. The surface impedance is complex in the general case of a lossy magneto-dielectric material. The additional to skin-depth surface impedance can be found by solving the rigorous boundary problem for surface, leaky, and bulk waves. This is a Sommerfeld-type problem, and the spectrum of modes is found from the solution of the complex-value transcendental equation [28].

Then this surface impedance is related to the total loss for the main propagating wave, for example, TEM mode on a coaxial line, or the quasi-TEM in a microstrip line. This problem formulation is illustrated by Figure 1.

The total surface impedance is comprised of two terms,

$$Z_s = R_s(1+j) + Z_{s1}, \tag{1}$$

where the first term, $Z_s = R_s(1+j)$, is associated with skin-effect, and the second, Z_{s1}, is the surface impedance due to the absorbing layer-air boundary, where surface waves propagate. Surface resistance R_s depends on the bulk conductivity σ of the metallic material,

$$R_s = \frac{1}{\sigma\delta_{skin}} = \sqrt{\frac{\omega\mu_0}{2\sigma}} \propto \sqrt{\omega}. \tag{2}$$

As is shown in [28, 29], the surface impedance Z_{s1} is associated with the propagating TM_z mode along the infinite planar structure.

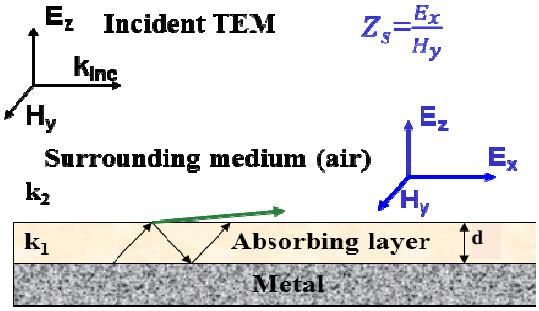

Figure 1. Surface impedance approach to characterize conductivity degradation of the metallic surface coated with magneto-dielectric absorbing layer.

This surface impedance can be calculated as

$$Z_{s1} = Z_{TM_z} = j\frac{\sqrt{(\omega/c)^2 \cdot \tilde{\mu}_r\tilde{\varepsilon}_r - \kappa_0^2}}{\omega\varepsilon_0\tilde{\varepsilon}_r} \tan\left(d \cdot \sqrt{\kappa_0^2 - (\omega/c)^2 \cdot \tilde{\mu}_r\tilde{\varepsilon}_r}\right), \quad (3)$$

where κ_0 is found as the lowest solution of the transcendental equation for the propagation constant κ and corresponds to the TM_z mode similar to [26]

$$\sqrt{\kappa^2 - (\omega/c)^2} = \frac{j\sqrt{\kappa^2 - (\omega/c)^2 \cdot \tilde{\mu}_r\tilde{\varepsilon}_r}}{\tilde{\varepsilon}_r} \cdot \tan\left(d \cdot \sqrt{\kappa^2 - (\omega/c)^2 \cdot \tilde{\mu}_r\tilde{\varepsilon}_r}\right)$$
$$\Rightarrow \kappa = \kappa_0. \quad (4)$$

This equation is obtained from matching the corresponding vector potentials at the boundaries metal-absorbing layer, and absorbing layer-air [27]. The corresponding wave numbers for the TEM waves are $k_1 = \omega\sqrt{\tilde{\mu}_r\tilde{\varepsilon}_r}/c$ inside the absorbing layer with relative complex permeability $\tilde{\mu}_r$ and permittivity $\tilde{\varepsilon}_r$, and $k_2 = \omega/c$ in the air. Thickness of the thin layer is d, as is seen from Figure 1. If $\kappa_0^2 \ll k_1^2$, the TMz wave, whose wave vector is directed normal to the surface plane, will propagate [27, Section 4.9], and an approximate formula for absorber-related surface impedance is nothing more than the input impedance of a metal-backed magneto-dielectric layer for a normally incident plane wave,

$$Z_{s1} = Z_{TM_z} \approx j\sqrt{\frac{\tilde{\mu}_r}{\tilde{\varepsilon}_r}} \cdot \sqrt{\frac{\mu_0}{\varepsilon_0}} \cdot \tan\left(\frac{\omega}{c} \cdot d \cdot \sqrt{\tilde{\mu}_r\tilde{\varepsilon}_r}\right). \quad (5)$$

As follows from (5), this impedance is complex in the general case of a lossy absorbing coating,

$$Z_{s1} = R_{s1} + jX_{s1}. \quad (6)$$

Then the total surface impedance (1) can be used to determine the parameter, which is called "surface displacement" [23]. The surface displacement is calculated as

$$D_s = \frac{Z_s}{j\omega\mu_0} \Rightarrow D_s = D'_s - jD''_s. \tag{7}$$

Its imaginary part D'' affects the total conductor loss on the transmission line with the coated conductor,

$$\alpha_c = \alpha_{c0} \cdot \frac{2D''_s}{\delta_{skin}}, \tag{8}$$

where α_{c0} is the initial conductor loss on the same line with the uncoated conductor. The total loss in the coaxial line is calculated as [30]

$$\alpha = \sqrt{\frac{1}{2}\left(R_{pul}G_{pul} - \omega^2 L_{pul}C_{pul}\right) + \frac{1}{2}\sqrt{\left(R^2_{pul} + \omega^2 L^2_{pul}\right)\left(G^2_{pul} + \omega^2 C^2_{pul}\right)}}. \tag{9}$$

where R_{pul}, L_{pul}, G_{pul}, and C_{pul} are the per-unit-length resistance, inductance, conductance, and capacitance, respectively. For the air-filled lines with comparatively low loss over the operating frequency range,

$$R_{pul} \ll \omega L_{pul}, \quad G_{pul} \ll \omega C_{pul}, \tag{10}$$

and hence the propagation constant for the TEM mode along the line is

$$\beta = \beta_0 \left[1 + \frac{1}{8\omega^2}\left(\frac{R_{pul}}{L_{pul}} - \frac{G_{pul}}{C_{pul}}\right)^2\right], \tag{11}$$

with $\beta_0 = \omega/c$, where c is the light velocity in vacuum, and total loss on the line is

$$\alpha = \frac{R_{pul}}{2Z_{W0}} + G_{pul}Z_{W0}, \tag{12}$$

$Z_{W0} = \sqrt{\frac{L_{pul}}{C_{pul}}}$ is the characteristic impedance of the perfect lossless line. In the air-filled coaxial line with the uncoated central conductor, loss comes from the conductors, and can be calculated as

$$\alpha_{c0} = \frac{R_{pul}}{2Z_{W0}}. \tag{13}$$

The next step is to calculate the RLCG parameters in the coaxial line with the coated central conductor. The total surface impedance of the line with the coated central conductor can be represented as

$$Z_s = R_s(1+j) + R_{s1} + jX_{s1} = (R_s + R_{s1}) + j(R_s + X_{s1}). \tag{14}$$

The equivalent per-unit-length resistance of the coaxial line with the coated central conductor is

$$R^c_{pul} = \frac{1}{2\pi}\left(\frac{R_s + R_{s1}}{a} + \frac{R_s}{b}\right), \tag{15}$$

where a and b are the corresponding internal and external radii of the coaxial line conductors, as is seen in Figure 2.

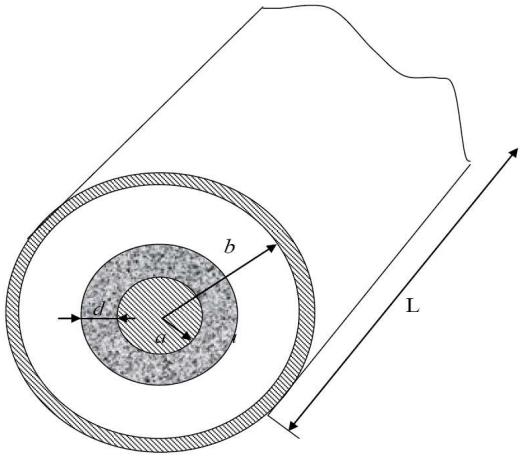

Figure 2. Geometry of the coaxial line with the coated central conductor.

The per-unit-length inductance of the line with the coated central conductor is

$$L^c_{pul} = \frac{\mu_0}{2\pi}\ln\left(\frac{b}{a}\right) + \frac{R_s + X_{s1}}{2\pi\omega \cdot a}. \tag{16}$$

Since the coating on the conductor is thin ($d \ll b$), per-unit-length capacitance and conductance in the line with the coated conductor remain the same as in the initial air-filled line.

$$C^c_{pul} = C_{pul} \approx \frac{2\pi\varepsilon_0}{\ln\left(\frac{b}{a}\right)} \text{ and } G^c_{pul} = G_{pul} \approx 0. \tag{17}$$

Then the per-unit-length parameters RLCG are used to calculate the corresponding S-parameters. This is done by calculating the complex propagation constant for the TEM mode in the line with the coated central conductor

$$\gamma = \sqrt{\left(R^c_{pul} + j\omega L^c_{pul}\right)\left(G^c_{pul} + j\omega C^c_{pul}\right)} = \alpha + j\beta, \tag{18}$$

and the corresponding complex characteristic impedance of the line is

$$Z_W = \sqrt{\left(R^c_{pul} + j\omega L^c_{pul}\right) / \left(G^c_{pul} + j\omega C^c_{pul}\right)} = |Z_W|\, e^{j\Phi_W}. \quad (19)$$

If the line is air-filled, then the loss comes from the coated conductor only, $\alpha = \alpha_c$,

$$\alpha_c = \mathrm{Re}\left(\sqrt{\left(R^c_{pul} + j\omega L^c_{pul}\right) j\omega C^c_{pul}}\right). \quad (20)$$

Then the ABCD matrix parameters [31]

$$\begin{bmatrix} A & B \\ C & D \end{bmatrix} = \begin{bmatrix} \cosh(\gamma L) & Z_W \sinh(\gamma L) \\ \sinh(\gamma L)/Z_W & \cosh(\gamma L) \end{bmatrix} \quad (21)$$

should be calculated and related to the S-parameters for the line section as [31]

$$\begin{bmatrix} S_{11} & S_{12} \\ S_{21} & S_{22} \end{bmatrix} = \begin{bmatrix} \frac{A+B/Z_W-CZ_W-D}{A+B/Z_W+CZ_W+D} & \frac{2(AD-BC)}{A+B/Z_W+CZ_W+D} \\ \frac{2}{A+B/Z_W+CZ_W+D} & \frac{-A+B/Z_W-CZ_W+D}{A+B/Z_W+CZ_W+D} \end{bmatrix}. \quad (22)$$

In the well-calibrated coaxial structure, when port effects are removed by the proper calibration procedure, the insertion loss (IL), which is the same as the magnitude of the transmission coefficient through the line $\left|S^{dB}_{21}\right|$, but with the opposite sign, can be calculated as

$$\left|S^{dB}_{21}\right| = -IL = -8.686\alpha_c \cdot L, \quad (23)$$

where L is the line length, and α_c is calculated for the line with the coated central conductor as (20). This calculated transmission coefficient will be compared with the experimental data and then with full-wave numerical simulations.

3. EXPERIMENTAL STUDY AND COMPARISON WITH THE ANALYTICAL MODEL

A few test flexible sheet absorbing materials were studied. Their dielectric and magnetic properties over the frequency range of interest were measured using the standard *Agilent* technique and software for material parameters extraction [20]. The picture of the experimental setup for measuring complex permittivity and permeability of the sample in the shape of washers is shown in Figure 3. A washer under test are placed inside the 7/3 mm coaxial airline between the inner and outer conductors, and the washer's plane is perpendicular to the

coaxial line axis. Five samples of different commercially available, e.g., NEC-Tokin, thin sheet magneto-dielectric composite materials with an adhesive layer to place upon a metal surface have been studied (see Table 1). Their compositions are unknown, but they all contain magnetic platelets in a polymer base. Their measured permittivity and permeability characteristics are shown in Figure 4 (Test Materials 1, 2, and 3) and Figure 5 (Test Materials 4 and 5). The observed resonances on the curves for Test Materials 1, 2, and 4 are most likely due to the resonance associated with the standing wave within the thickness of the test washers. This is seen from the shifts of resonances to the lower frequencies as thickness, relative permittivity, and relative permeability of the materials increase. In the thinner samples (Test Materials 2 and 4, $d = 0.1\,\text{mm}$), not quite smooth frequency responses of μ and ε can be observed, because the samples may slightly bend when placing into the coaxial line. At the same time, the material properties of samples are also frequency-dispersive. Dielectric properties of the material should be fairly smooth

Table 1. Test materials under study.

	Test Material 1	Test Material 2	Test Material 3	Test Material 4	Test Material 5
Sample Name	CA-19	EFR-01	EFR-03	FK2-01	FK2-05
Thickness, mm	0.15	0.1	0.3	0.1	0.5

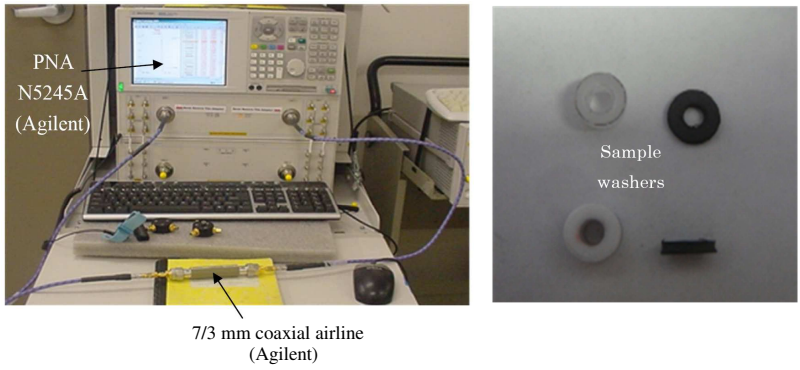

Figure 3. Experimental setup and samples (washers) for measuring dielectric and magnetic properties of absorbing materials.

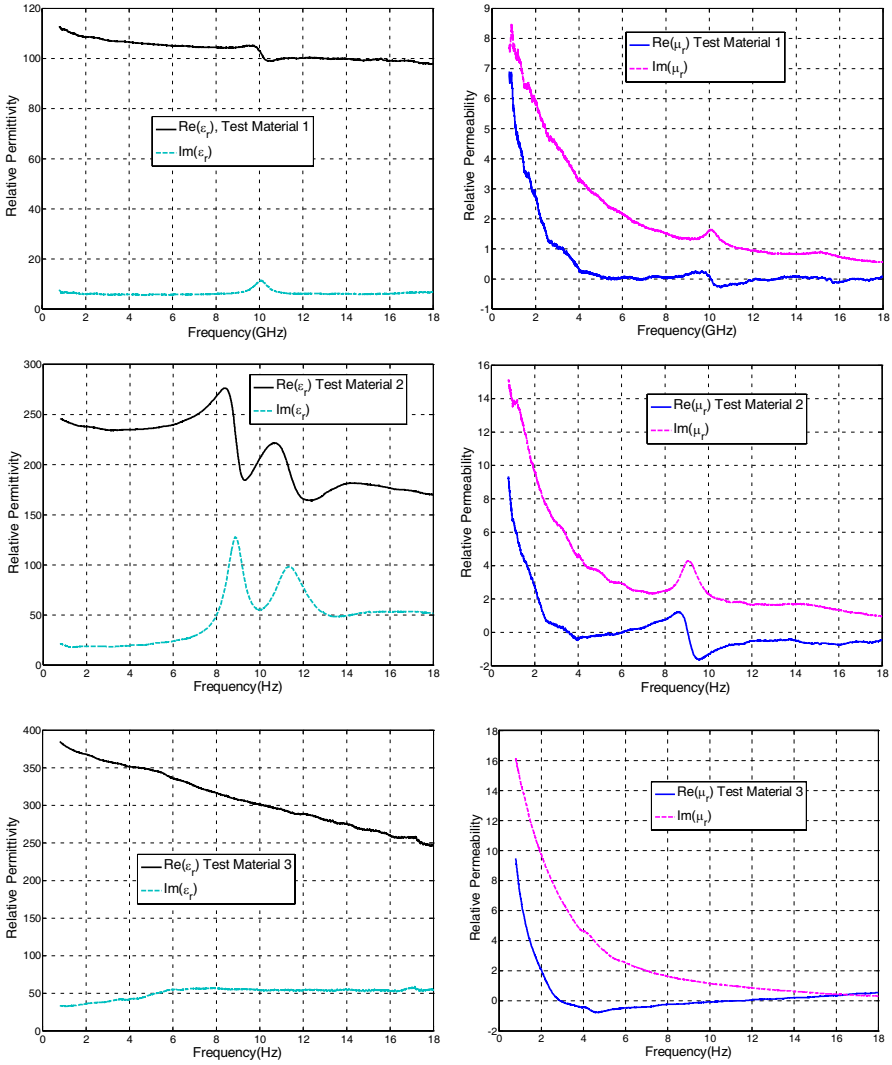

Figure 4. Frequency characteristics of permittivity and permeability of Test Materials 1, 2 & 3.

in the frequency range of measurements, while magnetic properties may exhibit the domain-wall or spin resonances ($\mu' < 0$ in some regions).

The measured frequency characteristics of the material samples were used in the analytical modeling as described in Section 2.

The results of the analytical modeling (magnitude of the insertion

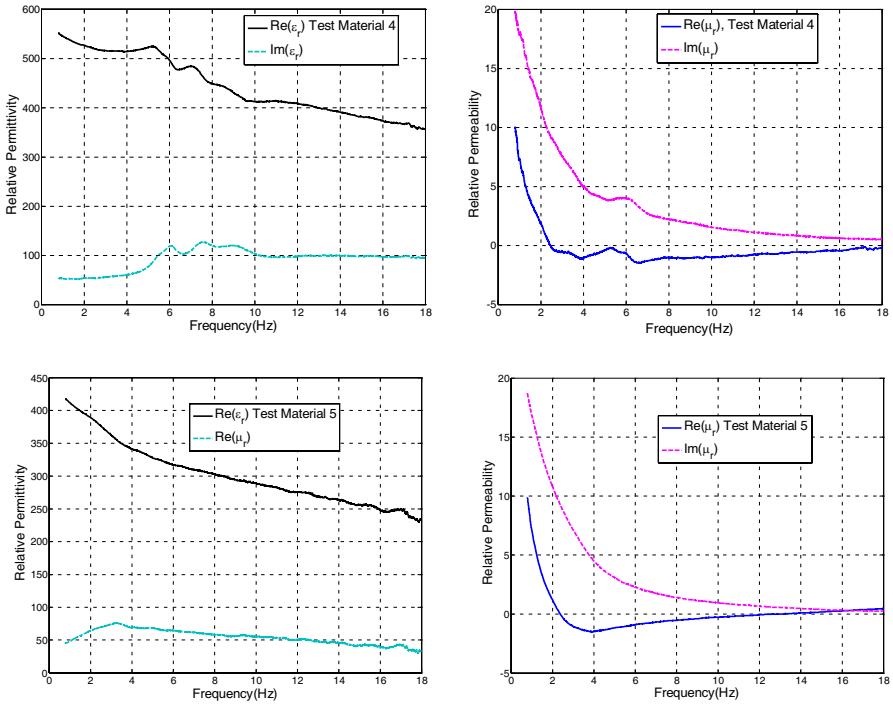

Figure 5. Frequency characteristics of permittivity and permeability of Test Materials 4 and 5.

loss) were compared with the measurement results, which were obtained by measuring the attenuation along the 7/3-mm coaxial airline (Agilent) of the length $L = 10\,\text{cm}$. The central conductor of the airline wrapped by a strip of the absorbing material. Figure 6 shows two test airlines (Agilent and Maury Microwaves), a central conductor of one of them, and a strip of the absorbing flexible magneto-dielectric material that will wrap the central conductor.

The analytically modeled and measured amplitudes $\left|S_{21}^{dB}\right|$ for three different test samples are shown in Figures 7–11. It is seen that the modeled results agree well with the measured results, at least outside the regions, where resonances associated with thickness of samples take place. The agreement is good for the samples of thickness $d = 0.15$ (Test Material 1) and 0.3 mm (Test Material 3). The thinner samples with $d = 0.1\,\text{mm}$ (Test Materials 2 and 4) show more discrepancy at the higher frequencies. There are a few reasons for this. First, the accuracy of measuring dielectric and magnetic properties of thinner samples may suffer because they could be slightly bent when

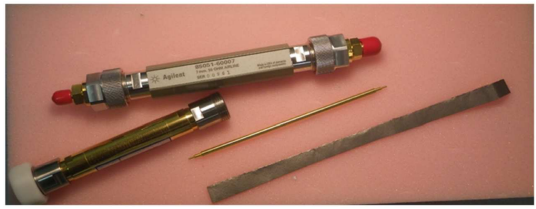

Figure 6. 7/3-mm airlines, a central conductor, and a strip of a flexible magneto-dielectric material under study.

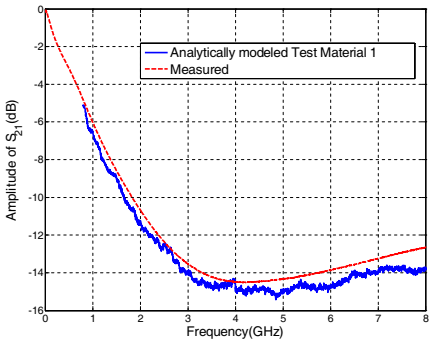

Figure 7. Measured and modeled loss in the line coated with Test Material 1 ($d = 0.15$ mm).

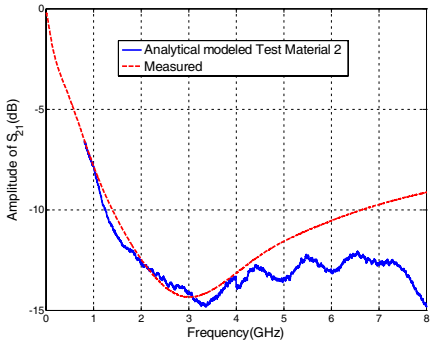

Figure 8. Measured and modeled loss in the line coated with Test Material 2 ($d = 0.1$ mm).

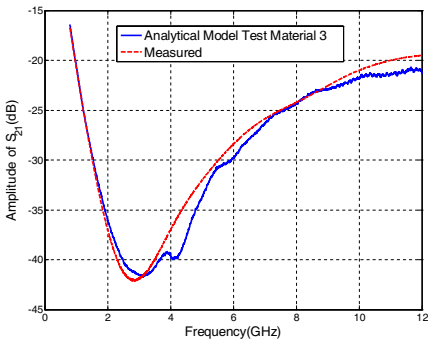

Figure 9. Measured and modeled loss in the line coated with Test Material 3 ($d = 0.3$ mm).

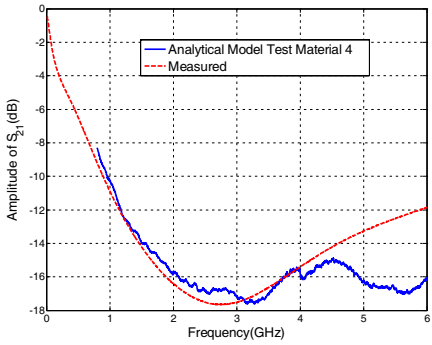

Figure 10. Measured and modeled loss in the line coated with Test Material 4 ($d = 0.1$ mm).

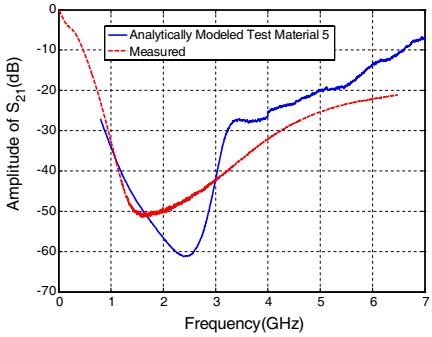

Figure 11. Measured and modeled loss in the line coated with Test Material 5 (d = 0.5 mm).

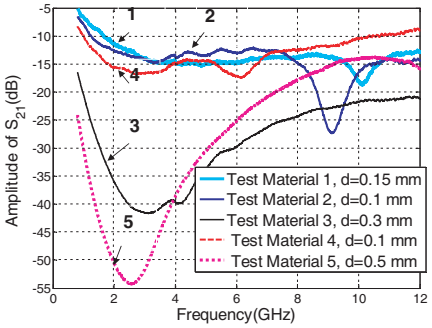

Figure 12. Comparison of the modeled attenuation on the line with different test materials.

placing inside the airline. Thicker samples, like Test Material 5 with $d = 0.5$ mm, shows large discrepancy over the whole frequency range. However, the thicker samples (Test Material 5) are more difficult to wrap around the conductor, and this may also cause the increased discrepancy. Also, when dealing with thicker samples, per-unit-length capacitance and conductance might be affected by the sample material. This may lead to the limitation in applicability of the concept of the surface impedance. From physics point of view, this is related to an excitation of higher-order surface and leaky modes in a layered structure, but in the presented model these modes are neglected. Thus the analytical model has been validated for the frequency range of 30 MHz to (8 . . . 12) GHz (comparatively low frequency range) and samples of test materials with the available thickness of 0.1, 0.15, and 0.3 mm (comparatively thin samples).

As soon as the analytical model is validated, it is possible to use it for predicting and comparing absorption efficiency of different materials and for different thicknesses, assuming that they are wrapped around the central conductor of the coaxial line. Figure 12 shows the comparison of attenuation on the line with five different test materials, the same as considered above. Figure 13 shows the predicted attenuation on the coaxial line if its central conductor were coated with the material with the same electromagnetic parameters as Test Material 3 (EFR-03), but with varying thickness of the layer in the range $d = 0.1 \ldots 0.35$ mm. It is seen from Figure 14 that the absorption on the line is almost linear with thickness. However, at higher frequencies, e.g., at the chosen for calculation frequency of 8 GHz,

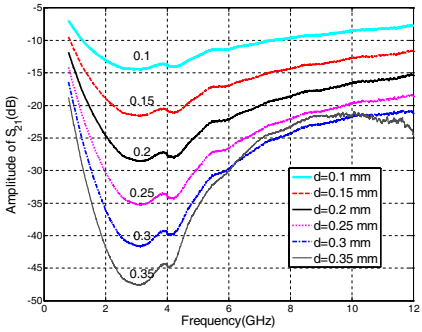

Figure 13. Predicted attenuation on the line with Test Material 3 of different thickness d.

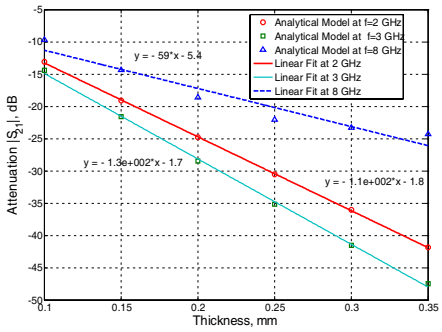

Figure 14. Predicted attenuation as the function of the thickness d of Test Material 3 for a few frequency points.

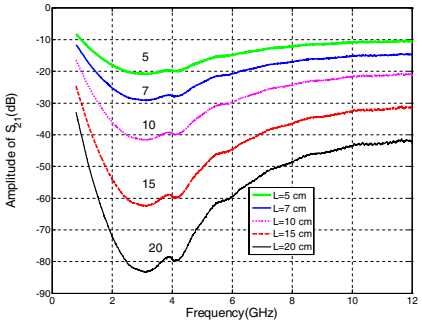

Figure 15. Predicted attenuation on the lines of different length L with Test Material 3.

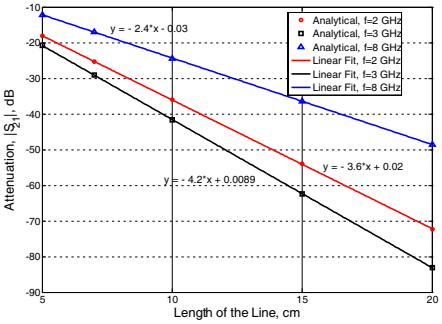

Figure 16. Predicted attenuation as a function of the line length with Test Material 3.

there is some deviation from linearity as thickness increases. However, dielectric and magnetic properties may be measured less accurately on a washer at higher frequencies. Moreover, as was shown above, for the thickness of the layer $d > 0.35$ mm, the analytical model may become inaccurate.

Figure 15 show the attenuation on the lines of different length with the same coating material (EFR-03). The dependences obtained from the analytical model upon length are almost linear (Figure 16), though the slope changes with frequency. This is an expected result, since the line exhibits translational invariance.

4. NUMERICAL SIMULATIONS

The analytical and experimental results are compared with the corresponding results of numerical 3D full-wave simulations. For these purpose, the CST Microwave Studio finite-element method (FEM) solver is employed. Geometry of the model is presented in Figure 17. In this model, the cable length $L = 10\,\text{cm}$, inner conductor radius $a = 1.52\,\text{mm}$, and outer conductor radius $b = 3.5\,\text{mm}$. In the numerical experiments, the central conductor is coated with different materials of different thickness d according to the Table 1.

The numerical model setup has the following peculiarities. The waveguide ports adjacent to the ends of the line are used on the both sides of the coaxial cable for excitation and termination. Only one mode is taken into account at the excitation waveguide port. To provide the single TEM mode propagation along the structure in the simulations, the waveguide ports are isolated from the coating by reducing the coating length by $dL = 1.5\,\text{mm}$ on the both ends of the coaxial line. Numerical experiments have proven that over the frequency range of interest (up to 12 GHz) the skin effect in the coaxial cable conductor is negligible compared to the loss in the absorbing coating. For this reason, a PEC has been chosen for modeling both conductors, which reduces the computational resources. The PEC has also been used as a background material outside the waveguiding structure to avoid field leakage from the waveguide ports into the surrounding space. The adaptive tetrahedral mesh has been employed for the FEM simulations. The model setup was tested for convergence. Taking into account the symmetry of the problem, two perpendicular perfect magnetic conductor (PMC) planes, where the

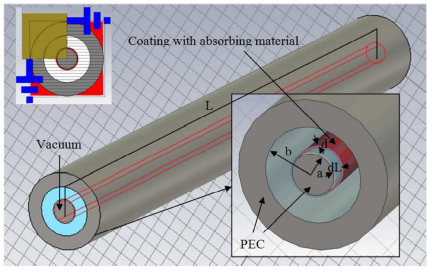

Figure 17. Numerical model setup.

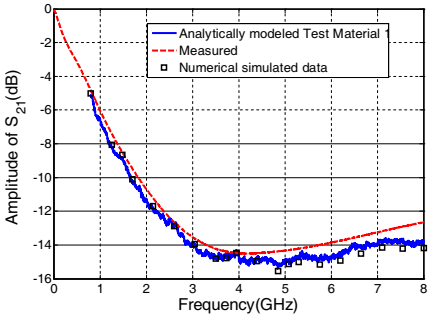

Figure 18. Analytical, measured, and numerical results for Test Material 1.

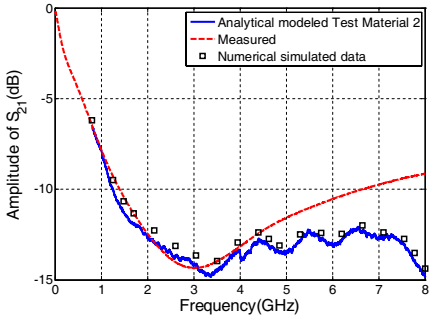

Figure 19. Analytical, measured, and numerical results for Test Material 2.

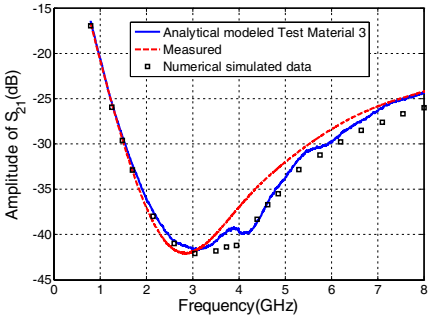

Figure 20. Analytical, measured, and numerical results for Test Material 3.

tangential component of the magnetic field is zero, were applied at the waveguide ports, as is shown in Figure 17. This allowed for considering just 1/4 of the problem, and thus decreasing the number of mesh cells by the factor of four.

The results of numerical simulations of the magnitude of S_{21} are presented along with the analytical and measurement results for Test Materials 1, 2, and 3, in Figures 18–20, respectively. It is seen that for all three samples, the agreement between the analytical and numerical models is excellent. The experimental results are the direct measurements of S_{21} on the line with the coated central conductor. In both analytical and numerical models the same input data for $\tilde{\mu}$ and $\tilde{\varepsilon}$ measured on the washers were used, even if these data are not quite accurate. This explains some discrepancy between the experimental and calculated results, especially at higher frequencies.

5. CONCLUSION

The analytical model to evaluate attenuation on the line with the central conductor coated with a magneto-dielectric layer is presented in this paper. It is validated by the experiments and numerical modeling in the frequency range of interest and for a number of the flexible absorbing sheet materials that could be wrapped around the central conductor of the testing coaxial line. It is shown that this model can be used for comparing absorptive effectiveness of different materials, as well as of different thicknesses and lengths of the same material. Another useful outcome of the proposed analytical model is that by solving an inverse problem, it is possible to retrieve permeability properties of an absorbing material. The inverse problem means that

the permeability as a function of frequency is reconstructed from the measured S-parameters. This procedure needs additional efforts in achieving accurate extraction of complex μ as a function of frequency, and this is a topic for a separate paper.

REFERENCES

1. Celozzi, S., R. Araneo, and G. Lovat, *Electromagnetic Shielding*, Wiley, New York, 2008.
2. Neelakanta, P. S., *Handbook of Electromagnetic Material: Monolithic and Composite Versions and Their Applications*, CRC Press, Boca Raton, FL, 1995.
3. Koledintseva, M. Y., J. Xu, S. De, J. L. Drewniak, Y. He, and R. Johnson, "Systematic analysis and engineering of absorbing materials containing magnetic inclusions for EMC applications," *IEEE Trans. Magn.*, Vol. 47, No. 2, 317–323, Feb. 2011.
4. Koledintseva, M., K. N. Rozanov, and J. L. Drewniak, "Engineering, modeling and testing of composite absorbing materials for EMC applications," *Advances in Composite Material — Ecodesign and Analysis*, B. Attaf (ed.), Chapter 13, 291–316, InTech, Mar. 2011.
5. Naito, Y. and K. Suetake, "Application of ferrite to electromagnetic wave absorber and its characterization," *IEEE Trans. Microw. Theory Techn.*, Vol. 19, 65–72, Jan. 1971.
6. Shin, J. Y. and J. H. Oh, "The microwave absorbing phenomena of ferrite microwave absorbers," *IEEE Trans. Magn.*, Vol. 29, No. 6, 3437–3439, Nov. 1993.
7. Anantharaman, M., K. Malini, S. Sindhu, E. M. Mohammed, S. K. Date, S. D. Kulkarni, P. A. Joy, and P. Kurian, "Tailoring magnetic and dielectric properties of rubber ferrite composites containing mixed ferrites," *Bulletin of Materials Science*, Vol. 24, No. 6, 623–631, Dec. 2001.
8. Chung, Y.-C., D.-Y. Kim, and D.-C. Park, "Design of broadband electromagnetic absorber using NiZn/MnZn hybrid structure," *Proc. IEEE Symp. Electromag. Compat.*, 409–412, Austin, TX, Aug. 1997.
9. Kazantseva, N. E., J. Vilcakova, V. Kresalek, P. Saha, I. Sapurina, and J. Stejskal, "Magnetic behavior of composites containing polyaniline-coated manganese-zinc ferrite," *Journal of Magnetism and Magnetic Materials (JMMM)*, Vol. 269, No. 1, 30–37, Feb. 2004.
10. Bregar, V., "Potential application of composite with ferromag-

netic nanoparticles in microwave absorber," *IEEE Trans. Magn.*, Vol. 40, 1679–1684, 2004.

11. Musal, H. and H. Hahn, "Thin-layer electromagnetic absorber design," *IEEE Trans. Magn.,* Vol. 25, No. 5, 3851–3853, May 1989.
12. Maslovski, S. I., P. M. T. Ikonen, I. Kolmakov, S. A. Tretyakov, and M. Kaunisto, "Artificial magnetic materials based on the new magnetic particle: Metasolenoid," *Progress In Electromagnetics Research*, Vol. 54, 61–81, 2005.
13. Ott, H., *Noise Reduction Techniques in Electronic Systems*, Wiley, New York, 1988.
14. Paul, C. R., *Introduction to Electromagnetic Compatibility*, Wiley, New York, 1992.
15. Vinoy, K. J. and R. M. Jha, *Radar Absorbing Materials — From Theory to Design and Characterization*, Kluwer Academic Publishers, Boston, MA, 1996.
16. Koledintseva, M. Y., V. V. Bodrov, I. V. Sourkova, M. M. Sabirov, and V. I. Sourkov, "Unified spectral technique application for study of radiator behavior near planar layered composites," *Progress In Electromagnetic Research*, Vol. 66, 317–357, 2006.
17. Nicolson, A. M. and G. Ross, "Measurement of the intrinsic properties of materials by time domain techniques," *IEEE Trans. Instrum. Meas.*, Vol. 19, 377–382, Nov. 1970.
18. Weir, W. B., "Automatic measurement of complex dielectric constant and permeability at microwave frequencies," *Proc. IEEE*, Vol. 62, 33–36, Jan. 1974.
19. Baker-Jarvis, J., "Transmission/reflection and short-circuit line permittivity measurements," Technical Note 1341, Department of Commerce, NIST, US, Jul. 1990.
20. *Agilent 85071E Materials Measurement Software*, Agilent Technologies, Technical Overview, Application Note 5988-9472EN, 2006.
21. Tosaka, T., I. Nagano, S. Yagitani, and Y. Yoshimura, "Determining the relative permeability and conductivity of thin materials," *IEEE Trans. Electromag. Compat.*, Vol. 47, No. 2, 352–360, May 2005.
22. Chen, L. F., C. K. Ong, C. P. Neo, V. V. Varadan, and V. K. Varadan, *Microwave Electronics: Measurement and Materials Characterisation*, Wiley, England, 2004.
23. Sanderson, A. E., "Effect of surface roughness on propagation of the TEM mode," *Advances in Microwaves*, Vol. 7, 2–57, Academic Press, 1971.

24. Holloway, C. L. and E. F. Kuester, "Power loss associated with conducting and superconducting rough surfaces," *IEEE Trans. Microw. Theory Tech.*, Vol. 48, No. 10, 1601–1610, Oct. 2000.
25. Matsushima, A. and K. Nakata, "Power loss and local surface impedance associated with conducting rough interfaces," *Electronics and Communications in Japan*, Part 2, Vol. 89, No. 1, 2006, translated from *Denshi Joho Gakkai Ronbunshi*, Vol. J88-C, No. 7, 502–511, Jul. 2005.
26. Koledintseva, M., A. Koul, F. Zhou, J. Drewniak, and S. Hinaga, "Surface impedance approach to calculate loss in rough conductor coated with dielectric layer," *IEEE Symp. Electromag. Compat.*, 790–795, Fort Lauderdale, FL, Jul. 2010.
27. Markov, G. T., B. M. Petrov, and G. P. Grudinskaya, *Electrodynamics and Radio Wave Propagation*, Chapter 6.3, Sovetskoye Radio, Moscow, 1979 (in Russian).
28. Collin, R. E., *Field Theory of Guided Waves*, 2nd edition, Chapter 11, IEEE, Wiley, 1991.
29. Goubau, G., "Surface waves and their application to transmission lines," *J. Appl. Phys.*, Vol. 21, 119–1128, 1950.
30. Baskakov, S. I., *Radio Engineering Circuits with Distributed Parameters*, Vysschaya Shkola, Moscow, 1980 (in Russian).
31. Pozar, D. M., *Microwave Engineering*, 2nd edition, Chapter 3, Wiley, 1998.
32. Koledintseva, M. Y., J. L. Drewniak, T. P. van Doren, D. J. Pommerenke, M. Cocchini, and D. M. Hockanson, "Method of edge currents for calculating mutual external inductance in a microstrip structure," *Progress In Electromagnetic Research*, Vol. 80, 197–224, 2008.